

Geophysical Research Letters®

RESEARCH LETTER

10.1029/2022GL102320

Key Points:

- Experimentally based flow law for dislocation creep of calcic-amphibole-rich (80 wt.%) rocks
- A calcic-amphibole-rich deep crust supports the “channel flow” model in southern Tibet
- Experimental amphibole crystal preferred orientations (CPO) may explain deep crustal seismic anisotropy

Supporting Information:

Supporting Information may be found in the online version of this article.

Correspondence to:

J. F. Zhang and A. Tommasi,
jfzhang@cug.edu.cn;
andrea.tommasi@umontpellier.fr

Citation:

Wang, X., Zhang, J. F., Tommasi, A., Lopez-Sanchez, M. A., Jing, Z. C., Shi, F., et al. (2023). Experimental evidence for a weak calcic-amphibole-rich deep crust in orogens. *Geophysical Research Letters*, 50, e2022GL102320. <https://doi.org/10.1029/2022GL102320>

Received 29 NOV 2022

Accepted 26 JUL 2023

Author Contributions:

Conceptualization: J. F. Zhang, A. Tommasi
Data curation: X. Wang, M. A. Lopez-Sanchez, F. Shi, W. L. Liu, F. Barou
Formal analysis: X. Wang
Funding acquisition: J. F. Zhang
Investigation: X. Wang
Methodology: X. Wang, M. A. Lopez-Sanchez, F. Shi, W. L. Liu, F. Barou
Project Administration: J. F. Zhang
Software: X. Wang, A. Tommasi, M. A. Lopez-Sanchez
Supervision: J. F. Zhang, A. Tommasi
Visualization: X. Wang

© 2023 The Authors.

This is an open access article under the terms of the Creative Commons Attribution-NonCommercial License, which permits use, distribution and reproduction in any medium, provided the original work is properly cited and is not used for commercial purposes.

Experimental Evidence for a Weak Calcic-Amphibole-Rich Deep Crust in Orogenes



X. Wang^{1,2} , J. F. Zhang¹ , A. Tommasi³ , M. A. Lopez-Sanchez^{3,4} , Z. C. Jing² , F. Shi¹, W. L. Liu¹, and F. Barou³ 

¹State Key Laboratory of Geological Process and Mineral Resources, School of Earth Sciences, China University of Geoscience, Wuhan, China, ²Department of Earth and Space Sciences, Southern University of Science and Technology, Shenzhen, China, ³Géosciences Montpellier, CNRS & Université de Montpellier, Montpellier, France, ⁴Department of Geology, University of Oviedo, Oviedo, Spain

Abstract Amphibole-rich rocks constitute significant components of the mid- to lower continental crust, particularly in active orogens characterized with thick and hot crusts. Nevertheless, experimental data on their viscosity remain scarce. We conducted axial compression deformation experiments on synthetic amphibolites under temperature and pressure conditions resembling deep sections of overthickened crust. A novel flow law for a calcic-amphibole-rich rock (80% amphibole +20% garnet) in the dislocation creep regime is derived from these experiments. Contrary to common assumptions, our results reveal that calcic-amphibolite is 1–2 orders of magnitude weaker than plagioclase-rich amphibolite, granulite, or gabbro. A calcic-amphibole-rich, low viscosity deep crust may not only support the “channel flow” model proposed for the Tibetan Plateau but also explain the observed high crustal seismic anisotropy in the region.

Plain Language Summary The rarity of earthquakes despite strong deformation in the deep crust of mountain belts produced by continental collisions, such as the Himalayas, implies that the deep continental crust is rather weak, easily dissipating imposed stresses by ductile deformation. The major components of the orogenic lower crust are plagioclase, amphibole, pyroxene, and garnet. Experimental data on the ductile deformation of coarse-grained amphibole-rich rocks was until now missing. We present new deformation experiments, from which we derive a flow law for an amphibolitic aggregate (80% amphibole +20% garnet). These data show high volumes of amphibole should result in high ductility and, hence, low strength in the deep crust, which should be considered when modeling the mechanical behavior of the lower crust during continental collisional. An amphibole-rich deep crust also accounts for the high crustal seismic anisotropy in southern Tibet.

1. Introduction

Geological and geophysical evidence indicates that the deep crust in overthickened orogens is weak and intensively deformed, allowing for “channel flow” and aseismic deformation (Bai et al., 2010; Clark & Royden, 2000; Grujic et al., 2011). However, the cause of this low viscosity remains contentious. The deep crust is generally thought to be intermediate to mafic in bulk composition, similar to amphibolite- and granulite-facies metabasalts. It is usually considered to be nominally anhydrous and mainly composed of plagioclase-pyroxene granulite (Rudnick & Gao, 2014). In such granulites, plagioclase is the weakest major mineral phase (Dimanov, 2005; Rybacki & Dresen, 2000). Classical strength envelope calculations for the continental lithosphere assume that the lower crust’s strength is dominated by calcic plagioclase’s mechanical behavior (Bürgmann & Dresen, 2008; Kohlstedt et al., 1995). However, a highly inhomogeneous deep crust composition was also proposed even within a single tectonic setting (Hacker et al., 2015; G. Wang et al., 2021).

In orogens, the deep crust undergoes a series of deformation, metamorphic, and magmatic events during subduction and collision. Fluids released during subduction may hydrate the deep crust, resulting in the formation of amphibole-rich rocks (Shinevar et al., 2021). Fractional crystallization of hydrous basaltic magmas may also produce amphibole-rich cumulates (Zhang et al., 2022; Zhou et al., 2020). In the Tibetan Plateau, a deep lower crust composed dominantly of (garnet) amphibolite (Hou et al., 2017) may better explain the observed strong crustal seismic anisotropy (Huang et al., 2022; Li et al., 2020; Wu et al., 2019) than a granulitic lower crust. This interpretation is consistent with deep crustal xenoliths as well as exhumed lower crustal rocks with dominantly

Writing – original draft: X. Wang, J. F. Zhang, A. Tommasi

Writing – review & editing: X. Wang, J. F. Zhang, A. Tommasi, M. A. Lopez-Sanchez, Z. C. Jing, F. Shi, W. L. Liu

amphibole-rich compositions and strong deformation (Ji et al., 2015; X. Wang et al., 2021). Partial melting of (garnet) amphibolite may also explain the postcollisional adakite-like magmatism in the Tibetan Plateau (Wang et al., 2019). Hence, amphibole is likely an important constituent mineral in the deep crust of Tibetan-type orogens. Petrological models also suggest that amphibole may be the dominant phase in the deep early continental crust (Johnson et al., 2017).

Previous studies have greatly advanced our knowledge of the deformation mechanisms, crystal preferred orientations (CPO), and seismic properties of amphibolites with various amphibole and plagioclase contents. In naturally deformed amphibolite, amphibole usually displays strong CPO and SPO, while the plagioclase CPO is generally weak (Elyaszadeh et al., 2018; Li et al., 2020). TEM data suggest that amphibole predominantly undergoes dislocation creep on the [001](100) slip system in nature (Skrotzki, 1992). An early experimental study on single crystals demonstrated that amphibole is strong and primarily deforms through twinning (100) or (101) below 800°C (Rooney et al., 1975). Axial compression experiments on natural and synthetic amphibolites (~50% Amp + 50% Pl) at 650–950°C, 0.5–1.5 GPa show localized, semi-brittle deformation at all temperatures in the natural amphibolites (Hacker & Christie, 1990; Wilks & Carter, 1990). In contrast, synthetic samples display a transition from localized to homogeneous deformation as temperature increases and strain rate decreases (at 850°C and 10^{-4} s⁻¹, 750°C and 10^{-4} s⁻¹, 650°C and 10^{-6} s⁻¹, Hacker & Christie, 1990). In shear experiments on natural amphibolites at 1 GPa, 480–700°C, amphibole also underwent cataclastic flow; fracturing accompanied by grain rotation produced nevertheless strong amphibole CPO, which was proposed to account for seismic anisotropy observations in the deep crust (Ko & Jung, 2015). Despite these studies on amphibolites, quantifying the contribution of amphibole to the rheological strength of the lower crust remains challenging, as data on the rheology (flow laws) of coarse-grained amphibole-dominated rocks, which are likely to constitute substantial volumes of the deep crust of orogens, and deform ductilely by dislocation creep, are still lacking. Due to the analogous crystallographic parameters of calcic-amphibole and clinopyroxene, geodynamical models frequently assumed their rheological strengths to be similar and both superior to that of plagioclase (e.g., Shinevar et al., 2015). Nonetheless, this assumption is not substantiated by experimental data on the deformation of calcic-amphibole under deep-crustal temperature and pressure conditions.

To address this issue, we have conducted axial compression experiments on hot-pressed polycrystalline aggregates composed of 80 wt. % calcic-amphibole (pargasite in Table S1 in Supporting Information S1) and 20 wt. % garnet with average grain sizes ranging from 30 to 75 μm at temperatures of 750–1,050°C, confining pressures of 1.8 GPa, and constant strain rates varying from 1.0×10^{-4} s⁻¹ to 6.0×10^{-6} s⁻¹. To assess the influence of mineral mode on amphibolite rheology, we also performed experiments on polycrystalline aggregates comprising either 100% amphibole or 50% amphibole +50% plagioclase. All experiments were performed in a 5 GPa modified Griggs deformation apparatus. The experimental conditions and mechanical data are summarized in Table S2 in Supporting Information S1. After the experiments, samples were cut and polished for microstructure measurement. Examination of the microstructures and CPO of the deformed specimens facilitated the characterization of prevailing deformation mechanisms in each mineral and elucidated the variations in strength. See Texts S1 and S2, Figures S1–S3 in Supporting Information S1 for experimental details and analytical methods.

2. Results

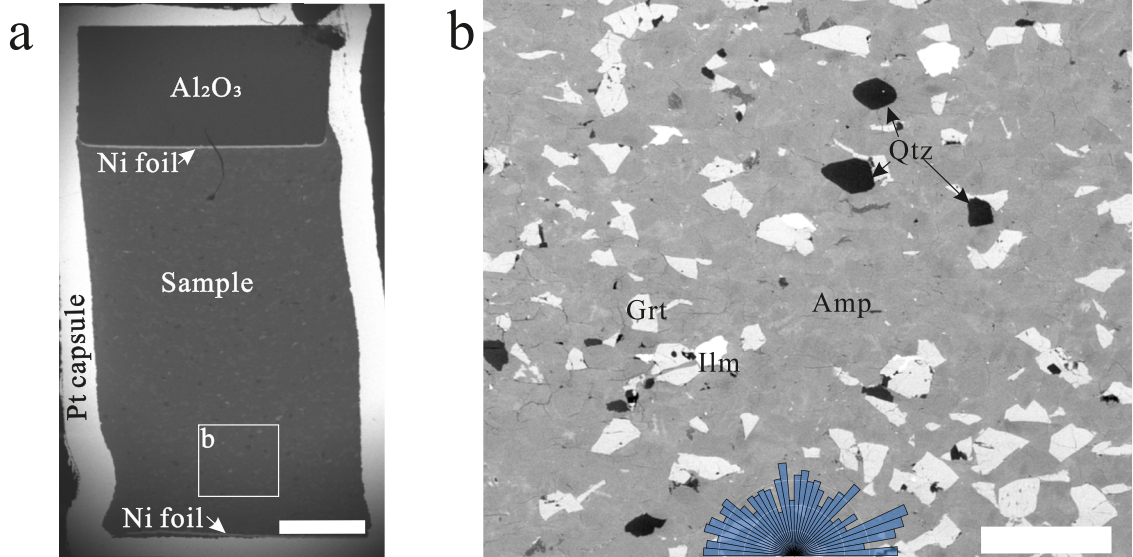
2.1. Initial (Hot-Pressed) Microstructure

SEM observations and EBSD mapping of the hot-pressed samples reveal a nearly homogeneous initial microstructure with average grain size of 39 μm for amphibole and 48 μm for garnet, respectively (Figures 1a and 1b and Table S3 in Supporting Information S1). Amphibole, garnet, minor quartz (~1%), and ilmenite (<1%) grains of angular shapes are distributed uniformly throughout the samples. Garnet shows little or no evidence of deformation. Amphibole displays a weak SPO and CPO indicating partial alignment of anisometric grains during hot-pressing (cf. rose diagram in Figure 1b and Figure S5a in Supporting Information S1). The axial compression ratio of three hot-pressed samples is quite similar, ranging from 33% to 34% (Table S2 in Supporting Information S1).

2.2. Deformation Microstructures

Deformed samples exhibit a pronounced foliation normal to the shortening direction marked by flattened amphibole (cf. rose diagram in Figure 1d), quartz, and ilmenite grains (Figures 1c and 1d). Amphibole has weak but

Hot-pressed experiment



Axial compression experiment

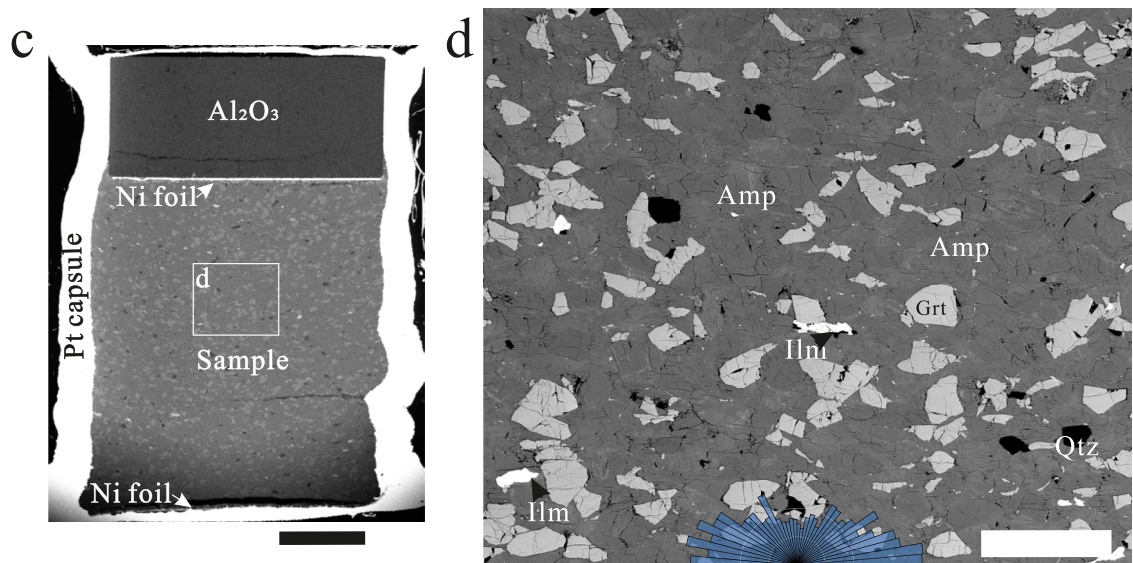


Figure 1. SEM images of representative hot-pressed and axial compression samples. The samples are welded in a platinum capsule (9 mm long, 3.2 mm inner diameter). A 1.4 mm Al₂O₃ piston is placed on top of the sample to protect it during capsule welding. Ni foils (25 µm) are placed on the top and bottom of the sample to control oxygen fugacity. (a) Specimen from hot-pressing experiment (GA286). (b) Enlarged image of the area highlighted in (a). (c) Specimen from axial compression experiment (GA351). (d) Enlarged image of the area highlighted in (c). The rose diagrams in b and d show the angular distribution of amphiboles long axis; the compression axis is at 90°. Mineral abbreviations: grt, garnet; amp, amphibole; qtz, quartz; ilm, ilmenite. Scale bar: 1 mm (a, c); 200 µm (b, d).

clear CPO marked by alignment of [100] in the compression direction and [001] normal to it (Figure 2b; Figures S5b–S5m in Supporting Information S1). Garnet has angular shapes similar to that in hot-pressed samples, no obvious elongation, and random orientations (Figure 2b), suggesting it behaved as rigid bodies within the matrix of deforming amphibole.

Phase boundaries and triple junctions in samples deformed at temperatures $\leq 900^{\circ}\text{C}$ are clear-cut and devoid of amorphous phases indicating partial melting, even at high magnification (Figure S4 in Supporting Information S1). The SEM images do not display compositional zoning within plagioclase and hornblende (Figure S4b in Supporting Information S1). Small amounts of amorphous material and newly formed garnet rims were only

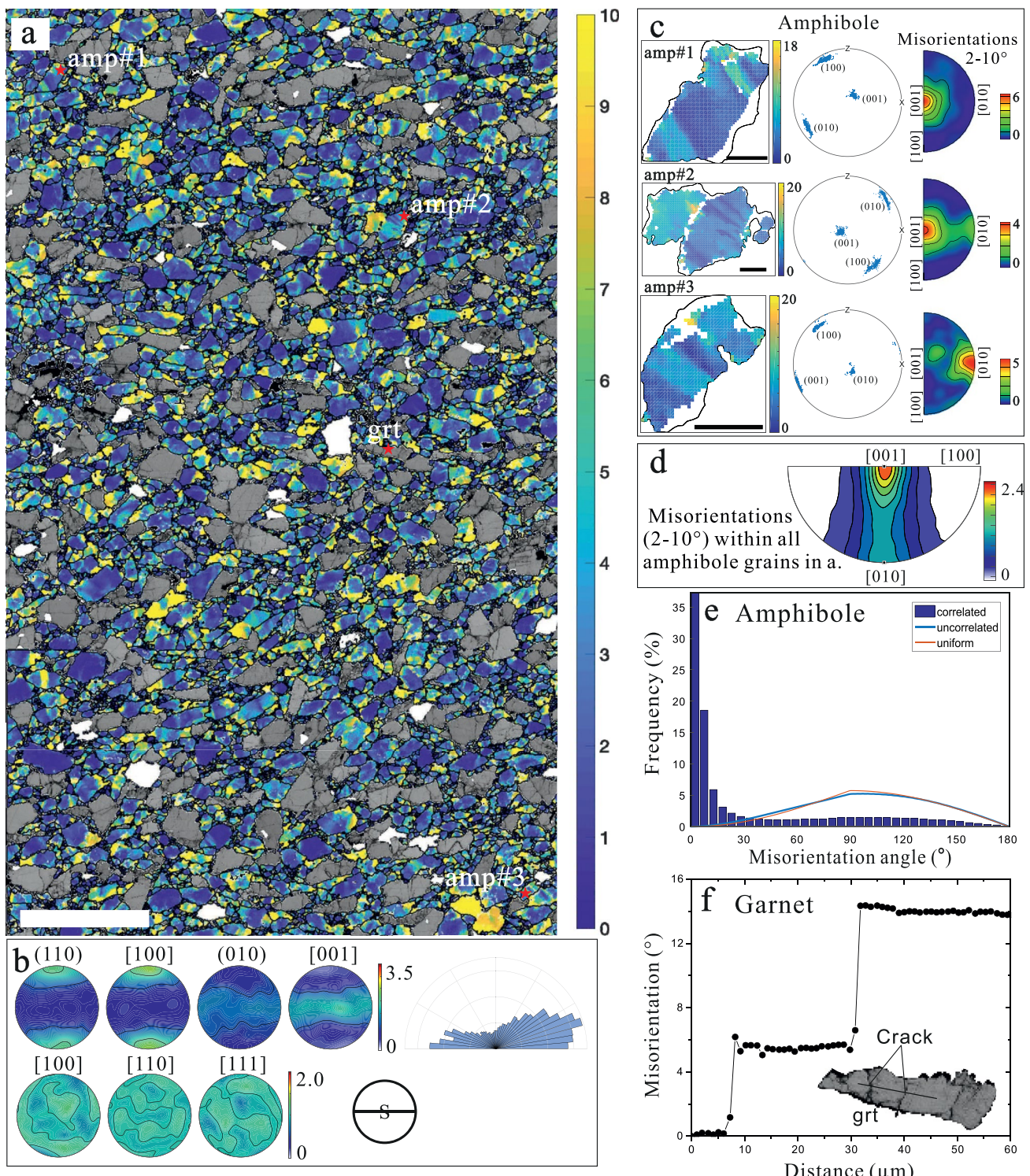


Figure 2.

observed in two samples deformed at 950°C and 1,050°C (GA288, 950°C; GA320, 1,050°C; Figures S4e and S4f in Supporting Information S1); these samples were excluded from the calculation of the flow law.

The CPO of amphibole, garnet, and plagioclase of all samples are displayed as pole figures in Figure S5 in Supporting Information S1. Amphiboles in all deformed samples show similar CPO despite varying experimental conditions: the [100] axes and, to a lesser extent, the poles of (110) align parallel to the compression direction and the [001] axes are distributed in a girdle on the foliation plane, normal to the compression direction (Figure 2b). Garnet displays almost random CPO (J close to 1) in all samples. Plagioclase develops a girdle distribution of the [100] axes on the foliation plane and a weak alignment of the (010) planes with the foliation.

These observations are corroborated by quantitative analysis of the microstructure based on high-resolution EBSD maps (step size = 0.4–1.3 μm) covering large areas ($\sim 1 \text{ mm} \times 3 \text{ mm}$) of deformed samples. Given that accumulation of dislocations produces distortion of the crystal lattice, to access the importance of dislocations in strain accommodation, we quantified the intragranular misorientations in the different phases by four parameters: the grain orientation spread (GOS), the misorientation of each pixel composing a grain relative to the mean orientation of the grain (M2M), the kernel average misorientation (KAM), which is the misorientation of each pixel composing a grain relative to the neighboring pixels within the grain, and the rotation axes accommodating these misorientations (in the crystal reference frame). Amphibole shows significantly higher average GOS than plagioclase or garnet (Table S3 in Supporting Information S1). In garnet grains, steps in misorientation profiles correlate with cracks (Figure 2f). In contrast, both amphibole and plagioclase display crystallographically controlled rotations accommodating intragranular misorientations, which are dominantly [001] and to a lesser extent [010] in amphibole and [100] in plagioclase (Figures 2c and 2d and Figure S6 in Supporting Information S1). Analysis of the subgrain boundaries, KAM, and M2M maps (Figure 2a and Figure S7 in Supporting Information S1) shows that the spatial distribution of intragranular misorientation in amphibole is highly heterogeneous both between grains and within grains, being usually higher in the vicinity of phase boundaries. In amphibole, planar deformation bands and subgrain boundaries are observed (Figure 2c). The histogram of misorientation angles of amphibole (at the sample scale) shows a high proportion of intragranular misorientations ($< 10^\circ$) and the absence of (100) twinning (Figure 2e and Figure S8 in Supporting Information S1). Both GOS and M2M values in amphibole decrease with increasing temperature (Table S1 in Supporting Information S1), consistent with more effective recovery at higher temperatures. Average amphibole grain sizes weighted by grain area of deformed samples are slightly smaller than those in the hot-pressed samples (Table S3 in Supporting Information S1).

2.3. Experimental Flow Law for an Amphibolite Composed of 80 wt. % Amp + 20 wt. % Grt

The mechanical data for the deformation experiments conducted at temperatures of 750–900°C, confining pressures of 1.8 GPa, and constant strain rates of $1.0 \times 10^{-4} \text{ s}^{-1}$ – $6.0 \times 10^{-6} \text{ s}^{-1}$ are displayed in Figure 3 and Table S2 in Supporting Information S1. As common for ductile deformation, decreasing the imposed strain rate or increasing the temperature results in decrease of the sample strength (Figure 3). Maximum stresses in most experiments are achieved between 0.15 and 0.20 of total shortening. Limited strain softening is observed in experiments with high flow stresses ($> 900 \text{ MPa}$). This softening is often observed in high-pressure deformation experiments and generally attributed to microstructure evolution or inhomogeneous deformation and specimen misalignment at large strains. Thus, the peak stress is taken as the flow stress to fit the constitutive equation.

The rheology of garnet amphibolite over the range of conditions explored can be described by the following constitutive equation obtained by a global fit to all data (Figures 3b and 3c):

$$\dot{\varepsilon} = A\sigma^n \exp\left(-\frac{Q}{RT}\right) = 10^{-6.2 \pm 0.7} \sigma^{3.1 \pm 0.4} \exp\left(-\frac{154 \pm 35 \text{ kJ/mol}}{RT}\right) \quad (1)$$

Figure 2. Intracrystalline deformation analysis of amphibole and garnet in representative sample GA458. (a) Amphibole intracrystalline misorientation map (blue to yellow colors indicate the misorientation relative to the mean orientation of the crystal, M2M, a proxy for the dislocation density), garnet is displayed in gray. Red stars indicate three amphibole grains analyzed in detail in c and the garnet grain analyzed in e. (b) Crystal preferred orientations of amphibole and garnet. The rose diagram shows the angular distribution of amphibole long axis (SPO). Insert on the bottom right indicates the orientation of the structural reference frame (S is the foliation, which is normal to the imposed shortening). (c) Detailed misorientation maps of three amphibole grains illustrating deformation bands and subgrain walls normal to the elongation of the grain and the associated intragranular misorientation and rotation axes. (d) Inverse pole figure of the rotation axes accommodating misorientations across subgrain boundaries of 2–10° within all amphibole grains in (a). (e) Histogram of misorientation angles in amphibole (at the sample scale) showing the high frequency of subgrain boundaries (intragranular misorientations $< 10^\circ$) and absence of twinning. (f) Misorientation profile within a garnet grain showing misorientations related to cracks. Scale bars: 250 μm (a), 20 μm (c).

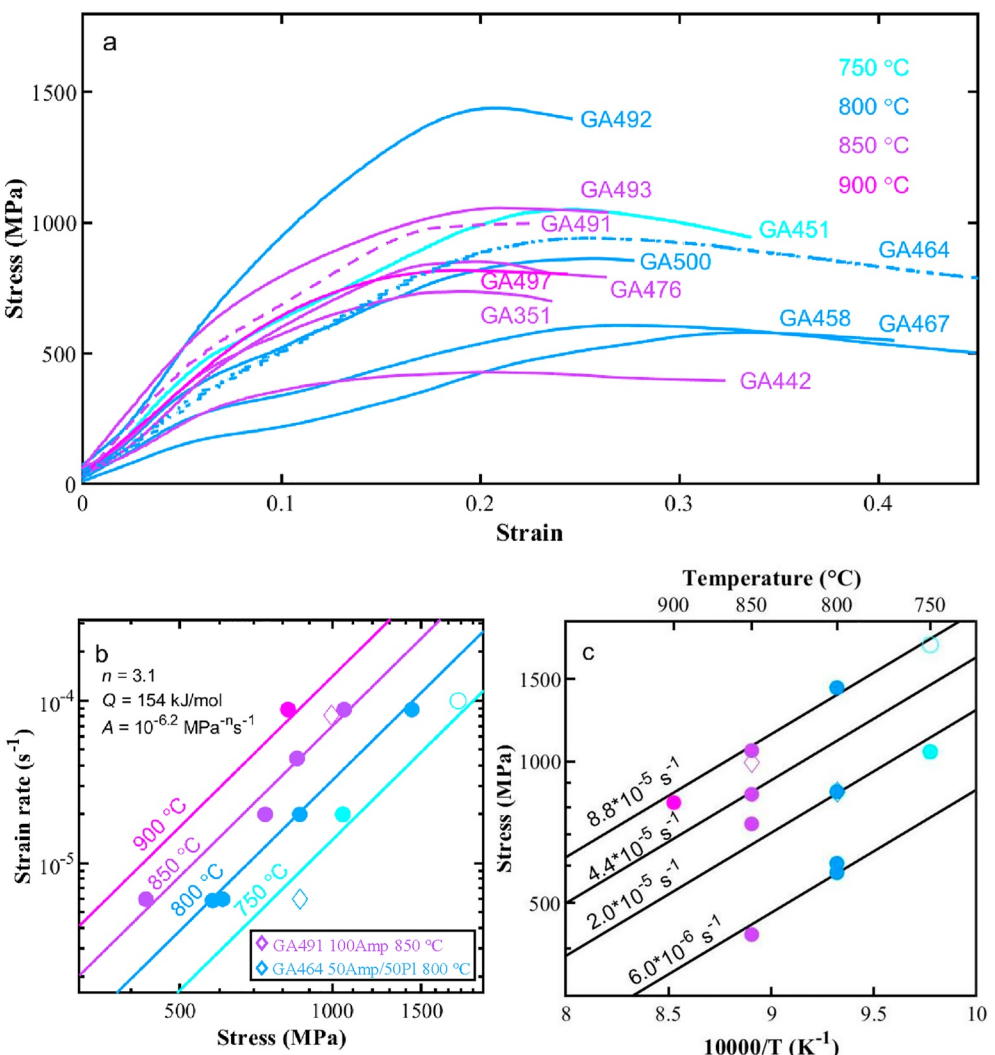


Figure 3. Mechanical data for high-temperature creep of amphibole-rich rocks. (a) Stress-strain curves of all experiments. The solid lines represent typical experiments on aggregates of 80% Amp + 20% Grt, while the dashed lines correspond to two distinct experiments on aggregates of 50% Amp + 50% Pl (GA464) and 100% Amp (GA491) compositions. Stress refers to differential stress ($\sigma_1 - \sigma_3$). (b) Strain rate versus average flow stress at 750°C, 800°C, 850°C, and 900°C. Empty circle indicates sample GA332, which was excluded from the definition of the flow law because it contained a crosscutting crack. (c) Flow stress (logscale) versus inverse temperature. Empty diamonds in (b and c) indicate sample GA464 and GA491. Full lines in (b and c) show the global fit to all data for 80% Amp + 20% Gt aggregates, which yield the n , Q , and A values in Equation 1.

where $\dot{\varepsilon}$ is the strain rate in s^{-1} , A is the pre-exponential factor, σ is the flow stress in MPa, n is the stress exponent, which depends on the deformation mechanism, Q is the activation energy in kJ/mol, R is the gas constant, and T is the absolute temperature.

2.4. Effect of the Mineral Mode

To test the effect of mineral mode on the strength of an amphibolite, we performed two additional experiments: one on a polycrystalline aggregate composed of 100% amphibole (GA491) at 850°C and another on a 50% amphibole +50% plagioclase ($\text{An}_{59}\text{Ab}_{40}$) aggregate (GA464) at 800°C (dashed lines in Figure 3a and empty diamonds in Figures 3b and 3c). The 100% amphibole aggregate (GA491) displays an average flow stress slightly lower than 20% Grt + 80% Amp aggregates (GA493) deformed at same conditions (997 MPa relative to 1,056 MPa; Figure 3b and Table S2 in Supporting Information S1). In contrast, the sample composed of 50% Pl ($\text{An}_{59}\text{Ab}_{40}$) + 50% Amp (GA464) displays approximately twice the strength of the 20% Grt + 80%

Amp aggregates (GA458&GA467) deformed at same conditions (average flow stress of 863 MPa relative to 580–607 MPa; Figure 3b; Table S2 in Supporting Information S1).

3. Discussion

3.1. Deformation Mechanisms

Early studies proposed a variety of mechanisms for producing CPO of amphibole based on observations of natural and experimental amphibole-rich rocks, including cataclastic flow at temperatures <650°C (Ko & Jung, 2015), diffusion creep in fine-grained aggregates developed in strain localization zones (Getsinger & Hirth, 2014; Mansard et al., 2020), dissolution-precipitation creep (Lee et al., 2022; Stokes et al., 2012), oriented synkinematic crystallization and growth (Mansard et al., 2020; Tommasi et al., 2017), and dislocation creep (Elyaszadeh et al., 2018; Skrotzki, 1992).

In the present study, both the deformation microstructures (clear foliation marked by flattened grains, well-developed CPO, intragranular misorientations with coherent rotation axes, frequent subgrain boundaries) and the measured stress exponent of $n = 3.1$ suggest that dislocation creep is the dominant deformation mechanism for amphibole. The CPO of amphibole is consistent with dominant activation of the [001](100) slip system. However, intragranular misorientations associated with rotations around [001] indicate that other slip systems were also active during deformation. These intragranular misorientations may be produced by accumulation of edge dislocations of the [100](010) and $1/2<110>\{110\}$ systems, which are secondary slip systems in amphibole (Skrotzki, 1992). The present observations are consistent with TEM data from a natural amphibolite deformed at temperatures >650°C (Skrotzki, 1992), which denoted deformation by dislocation creep with dominant activation of [001](100), secondary activation of [100](010) and $1/2<110>\{110\}$, and recovery by cross-slip of [001] screw dislocations and climb of [100] and $\frac{1}{2}<110>$ edge dislocations. Amphibole CPO and microstructures similar to those formed in the present experiments have been reported in the EI Rellano amphibolite from southwestern Spain (Díaz Aspiroz et al., 2007) and in deformed gabbro from Neyriz mantle diapir, Iran (Elyaszadeh et al., 2018), which were deformed at temperatures >840°C. It suggests that [001](100) is the dominant slip system in amphibole at temperatures >650°C over a wide range of pressure, at both the present laboratory and natural strain rate conditions, thus, at conditions, which encompass those expected in the deep crust of overthickened orogens.

The weak CPO and subgrains in plagioclase indicate limited deformation by dislocation creep with dominant activation of the [100](001) and [100](010) slip systems. Dominant [100] slip is consistent with observations implying that [100] is the slip direction most easily activated in plagioclase under high-temperature conditions (Ji et al., 2000). However, compared to amphibole, the less elongated shapes, lower intragranular misorientations, and weaker CPO of plagioclase suggest that plagioclase accommodated less strain than amphibole, consistent with the higher strength of the plagioclase-dominated assemblages relative to those composed mostly by amphibole.

The angular grain shapes and almost random CPO of garnet imply high strength, leading to solid grain rotation and translation in the present experiments. Cataclastic flow usually predominates in garnet under relatively low temperatures, high strain rate, and dry conditions (Zhang & Green, 2007). Deformation experiments on garnet single crystals only showed evidence for dislocation creep at temperatures $\geq 1,000^\circ\text{C}$ and wet conditions (Voegelé et al., 1998). In nature garnet may nevertheless deform ductilely at lower temperature (>600°C) due to much lower strain rates (Phillips & Ji, 2021).

3.2. Strength and Viscosity of an Amphibole-Rich Deep Crust

In Figure 4a and Figure S9 in Supporting Information S1, we compare the flow law for calcic-amphibole-rich rocks deduced from the present experiments with results of previous studies for lower crustal rocks with different mineral modes and water contents in a plot of temperature vs. flow stress for a fixed geological strain rate of 10^{-14} s^{-1} . The current findings indicate that, in the dislocation creep regime, the rheological strength of an amphibole-rich rock is 3–4 times inferior to that of a rock in which water-saturated plagioclase dominate, and 2–3 orders of magnitude weaker than that of a rock composed mainly by dry plagioclase and water-saturated clinopyroxene. The formation of amphibole, thus, considerably diminishes the rheological strength of mafic

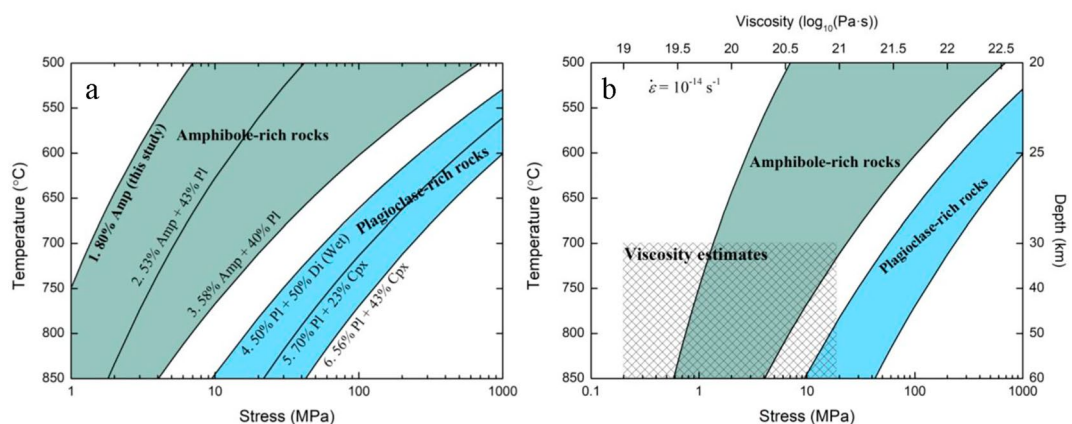


Figure 4. Flow strength comparison of amphibole-rich rocks and plagioclase-rich rocks. (a) Flow strength of amphibole-rich rocks (#1–#3), wet (#4) and dry (#5–#6) plagioclase-rich rocks in the dislocation creep regime derived by extrapolating flow laws to natural strain rate ($\dot{\epsilon}$) of 10^{-14} s^{-1} . Amphibole-rich rock (#2) refers to 53% Amp + 43% Pl ($\text{Ab}_{70}\text{An}_{30}$) (Hacker & Christie, 1990). Amphibole-rich rock (#3) refers to 58% Amp + 40% Pl ($\text{Ab}_{25}\text{An}_{75}$) (Wilks & Carter, 1990). Plagioclase-rich rock (#4) refers to water saturated 50% An + 50% Di, which is calculated by wet plagioclase and wet diopside using mixing model introduced by Huet et al. (2014) (Figure S9 in Supporting Information S1). Plagioclase-rich rock (#5) refers to 70% Pl ($\text{Ab}_{50}\text{An}_{50}$) + 23% Cpx (Mackwell et al., 1998). Plagioclase-rich rock (#6) refers to 56% Pl ($\text{Ab}_{50}\text{An}_{50}$) + 43% Cpx (Mackwell et al., 1998). (b) Comparison between crustal viscosity (η) in southern Tibet deduced from geodetic estimate (Chen et al., 2022; England et al., 2013; Henriet et al., 2019; Rippe & Unsworth, 2010; Ryder et al., 2014) and the viscosity of amphibole-rich rocks and plagioclase-rich mafic rocks derived from deformation experiments in dislocation creep regime. The viscosity is calculated as: $\eta = \sigma / (2 \times \dot{\epsilon})$. Strain rate ($\dot{\epsilon}$) is assumed as 10^{-14} s^{-1} . The depth is calculated based on the geothermal gradient from Hacker et al. (2014). Rheological parameters are summarized in Table S4 in Supporting Information S1.

rocks in the deep crust. Amphibole-plagioclase-rich amphibolites are 1–2 orders of magnitude weaker than plagioclase-pyroxene-rich granulites, contingent upon the content of amphibole and the hydration state of plagioclase. Several lines of evidence corroborate this conclusion: (a) The flow strength of amphibolite (53 wt. % Amp + 43 wt. % Pl ($\text{Ab}_{70}\text{An}_{30}$); Hacker & Christie, 1990) is lower than that of dry plagioclase aggregates in the dislocation creep regime (Rybacki & Dresen, 2000), which means that input of amphibole weakens the strength of plagioclase aggregates. (b) The strength of an amphibolite with 50 wt. % plagioclase ($\text{Ab}_{50}\text{An}_{40}$) is about two times stronger than that of the aggregate composed of 100% amphibole (Figure 3b). Overall, the strength as a function of modal composition varies as: amphibole-rich amphibolite [80% Amp < 43% Pl ($\text{Ab}_{70}\text{An}_{30}$) + 53% Amp < 40% Pl ($\text{Ab}_{25}\text{An}_{75}$) + 58% Amp] < wet plagioclase-pyroxene rocks (50% wet Pl + 50% wet Di) < dry plagioclase-pyroxene rocks [70% Pl ($\text{Ab}_{50}\text{An}_{50}$) + 23% Cpx < 56% Pl ($\text{Ab}_{50}\text{An}_{50}$) + 43% Cpx]. Garnet, in proportion of up to 20 wt. %, does not significantly increase the amphibolite strength (Figure 3b), as for such modal contents garnet behaves as non-connected rigid inclusions. Given its low ductility, higher garnet contents will probably result in a major increase in the rock strength.

In summary, the present mechanical data indicate that the strength of plagioclase is not suitable to represent the strength of continental deep crust if the latter contains large amounts of amphibole and deforms in the dislocation creep regime. Dislocation creep of amphibole may not be the main strain accommodation process in the lower crust when grain sizes are small or fluids, melt, or other weaker phases (quartz or mica) are present. However, the latter conditions are probably more often met in felsic rocks from shallow crustal depths than in mafic rocks from deep crustal levels of thickened orogenic belts and natural amphibolites usually have grain sizes of 0.2–2 mm, that is, two to three orders of magnitude coarser than those in diffusion creep experiments (grain sizes <10 μm).

3.3. Implications to the Southern Tibet Deformation

Based on these flow laws of Figure 4, we calculated the viscosity of Ca-amphibole dominated amphibolites and plagioclase-pyroxene granulites assuming a constant strain rate of 10^{-14} s^{-1} and compared our results with independent estimates of viscosity in the deep crust of southern Tibet derived from geodetic constraints based on post-seismic relaxation (Chen et al., 2022 [$\sim 10^{19} \text{ Pa}\cdot\text{s}$]; Ryder et al., 2014 [$6 \cdot 10^{19} \text{--} 10^{20} \text{ Pa}\cdot\text{s}$]) and paleolake

shoreline deformation (England et al., 2013 [10^{19} – 10^{20} Pa·s]; Henriet et al., 2019 [10^{20} – 10^{21} Pa·s]). Geodetic viscosity estimates for the deep crust of in southern Tibet range from 10^{19} to 10^{21} Pa·s. In all these studies, the deep crust is modeled as a single layer with uniform viscosity, these values are thus estimates of the average viscosity between 30 and 60 km (gray boxes in Figure 4b). The viscosity of amphibole-rich rocks matches well the viscosity of the southern Tibet crust at depths of 30–50 km while that of plagioclase-pyroxene granulites are 1–2 orders of magnitude higher. The higher viscosity inferred for the lowermost crust may result from increasing plagioclase contents or progressive replacement of amphibole by pyroxenes through dehydration.

The uplift of the Tibetan Plateau has been a hot topic over the past decades. Three main models have been proposed to account for it: thinning of thickened mantle lithosphere (Turner et al., 1996), intracontinental subduction (Tapponnier et al., 2001), and crustal channel flow (Royden et al., 1997). These models diverge on whether the deep crust and the upper mantle are strongly coupled or not. A weak deep crust in southern Tibet (Lhasa terrane) leading to crust-mantle decoupling is required by the “channel flow” model. A key difficulty in discriminating between these models is that the composition and the rheology of the deep crust are poorly constrained.

Magnetotelluric profiles of eastern Lhasa showed two major channels of high electrical conductivity at a depth of ~30–50 km (Bai et al., 2010). The rarity of seismicity at these depths compared to the upper crust and lowermost crust/upper mantle implies that this layer is weaker than the lowermost crust/upper mantle (Sloan et al., 2011). Partial melt may cause both high electrical conductivity and weakening. However, partial melting is probably very limited in the overthickened crust of southern Tibet, because temperatures inferred from geotherms (Wang et al., 2013) are lower than the solidus of amphibolite and mica-bearing rocks in deep crust (Figure S10 in Supporting Information S1). The present results imply that an amphibolitic deep crust will display low strength. Enhanced electrical conductivity of amphibole after dehydrogenation (Hu et al., 2018) may explain the observed high conductivity anomalies. Finally, water release from dehydration of metastable amphibole-rich rocks might explain earthquakes in the lowermost crust (50–70 km) of the Tibetan Plateau by a process similar to the dehydration embrittlement of hydrous minerals proposed for explaining intermediate-depth (50–300 km) earthquakes in subduction zones (Okazaki & Hirth, 2016).

Seismic anisotropy is a useful tool to probe the deformation in deep Earth, as it often results from CPO produced by ductile deformation. SKS waves have been widely applied to obtain mantle deformation patterns. P to S converted phases from the Moho have been used to study crustal anisotropy successfully (Liu & Niu, 2012). Strong crustal anisotropies have been observed in many orogens, like Tibet (Wu et al., 2019), the Andes (Moschetti et al., 2010), and the Aegean Sea (Endrun et al., 2011). The dominant minerals of the continental deep crust are pyroxene, plagioclase, amphibole, and garnet. The present and previous experimental data indicate that amphibole tends to develop strong CPO in response to deformation (Figure S5 in Supporting Information S1; Ko & Jung, 2015) and may therefore play a critical role in the formation of strong seismic anisotropy in the deep crust. The presence of plagioclase, pyroxene, and garnet dilutes the seismic anisotropy induced by amphibole CPO (X. Wang et al., 2021). Thus observation of a strong crustal anisotropy implies both coherent deformation and large contents of amphibole (or biotite) over length scales of tens of km in the deep crust (Li et al., 2020; Lloyd et al., 2009).

V_p , V_s , and V_p/V_s ratio are additional criteria for determining the composition of the deep crust. Nevertheless, because the main contrast between amphibolite and granulite stems from the replacement of pyroxene by amphibole, the weak contrasts in V_p and V_s between amphibole and pyroxene (Christensen, 1996; Kern et al., 1996), result in small variations in V_p/V_s ratio. It is, therefore, challenging to distinguish amphibole-plagioclase-rich amphibolite from plagioclase-pyroxene-rich granulite based on V_p , V_s , and V_p/V_s ratio.

In the present study, we show that amphibole is the weakest phase compared with plagioclase, pyroxene, or garnet in coarse-grained mafic rocks (e.g., granulite and eclogite). Under such conditions, which may have prevailed during the deformation of the Tibetan deep crust, amphibole will bear most strain and form strong CPOs that could explain the observed strong crustal seismic anisotropies. The high ductility of calcic-amphibole may also allow for mechanical decoupling between the upper crust and upper mantle or eclogitic lowermost crust within a collision zone (Royden et al., 1997).

4. Conclusions

This study presents, for the first time, quantitative data on the mechanical strength of calcic-amphibole-rich (80% pargasite) rocks in the dislocation creep regime and contrasts these findings with published flow laws for

amphibole-plagioclase rocks and plagioclase-pyroxene rocks with various plagioclase content. The outcomes indicate that a calcic-amphibole-rich deep crust may function as a weak layer in orogens. A calcic-amphibole-rich deep crust undergoing deformation by dislocation creep could support the “channel flow” model, potentially accounting for the low viscosity in the deep crust and crustal seismic anisotropy in southern Tibet. Consequently, the novel flow law of amphibole-rich composition ought to be considered when modeling the mechanical behavior of the lower crust. Microstructural analysis of the deformed amphibolites reveals that amphibole and plagioclase deformed dominantly by dislocation creep with dominant activation of the [001](100) slip system in amphibole and of [100](001)/[100](010) in plagioclase over a very wide range of temperature and strain rate conditions. Deformation of amphibole-rich rocks by dislocation creep produces strong amphibole CPO, which may explain seismic anisotropy measurements in the deep crust of orogenic belts.

Data Availability Statement

Data: The raw stress-strain data and EBSD data (CTF files) are available from the Figshare Repository: <https://doi.org/10.6084/m9.figshare.20227329>. **Software:** The publicly accessible MATLAB (MATLAB, 2021a) toolbox, MTEX, that was used to perform the analysis of EBSD data is openly available for download: <https://mtex-toolbox.github.io/>.

Acknowledgments

We are grateful to Chujian Liu for the fabrication of parts for sample assemblies. Wenjing Li and Zhonghang Wang are thanked for their guidance on HT/HP experiments and EBSD measurements. C. Nevado and D. Delmas prepared high-quality polished thin sections for EBSD measurements. This work was supported by the National Natural Science Foundation of China (Grant 42172250), the Postdoctoral Research Foundation of China (2021M701563), the MOST special fund from the State Key Laboratory of GPMR, and the Shenzhen Science, Technology and Innovation Commission Program (20220815114624002).

References

- Bai, D., Unsworth, M. J., Meju, M. A., Ma, X., Teng, J., Kong, X., et al. (2010). Crustal deformation of the eastern Tibetan plateau revealed by magnetotelluric imaging. *Nature Geoscience*, 3(5), 358–362. <https://doi.org/10.1038/ngeo830>
- Bürgmann, R., & Dresen, G. (2008). Rheology of the lower crust and upper mantle: Evidence from rock mechanics, geodesy, and field observations. *Annual Review of Earth and Planetary Sciences*, 36(1), 531–567. <https://doi.org/10.1146/annurev.earth.36.031207.124326>
- Chen, Y., Hu, Y., Qian, L., & Meng, G. (2022). Early Postseismic Deformation of the 2010 Mw 6.9 Yushu earthquake and its implication for lithospheric rheological properties. *Geophysical Research Letters*, 49(15), e2022GL098942. <https://doi.org/10.1029/2022gl098942>
- Christensen, N. I. (1996). Poisson's ratio and crustal seismology. *Journal of Geophysical Research: Solid Earth*, 101(B2), 3139–3156. <https://doi.org/10.1029/95jb03446>
- Clark, M. K., & Royden, L. H. (2000). Topographic ooze: Building the eastern margin of Tibet by lower crustal flow. *Geology*, 28(8), 703–706. [https://doi.org/10.1130/0091-7613\(2000\)028<0703:tobtem>2.3.co;2](https://doi.org/10.1130/0091-7613(2000)028<0703:tobtem>2.3.co;2)
- Díaz Aspiroz, M., Lloyd, G. E., & Fernández, C. (2007). Development of lattice preferred orientation in clinoamphiboles deformed under low-pressure metamorphic conditions. A SEM/EBSD study of metabasites from the Aracena metamorphic belt (SW Spain). *Journal of Structural Geology*, 29(4), 629–645. <https://doi.org/10.1016/j.jsg.2006.10.010>
- Dimanov, A. (2005). Rheology of synthetic anorthite-diopside aggregates: Implications for ductile shear zones. *Journal of Geophysical Research: Solid Earth*, 110(B7), 1–24. <https://doi.org/10.1029/2004jb003431>
- Elyaszadeh, R., Prior, D. J., Sarkarnejad, K., & Mansouri, H. (2018). Different slip systems controlling crystallographic preferred orientation and intracrystalline deformation of amphibole in mylonites from the Neyriz mantle diapir, Iran. *Journal of Structural Geology*, 107, 38–52. <https://doi.org/10.1016/j.jsg.2017.11.020>
- Endrun, B., Lebedev, S., Meier, T., Tirel, C., & Friederich, W. (2011). Complex layered deformation within the Aegean crust and mantle revealed by seismic anisotropy. *Nature Geoscience*, 4(3), 203–207. <https://doi.org/10.1038/ngeo1065>
- England, P. C., Walker, R. T., Fu, B., & Floyd, M. A. (2013). A bound on the viscosity of the Tibetan crust from the horizontality of palaeolake shorelines. *Earth and Planetary Science Letters*, 375, 44–56. <https://doi.org/10.1016/j.epsl.2013.05.001>
- Getsinger, A., & Hirth, G. (2014). Amphibole fabric formation during diffusion creep and the rheology of shear zones. *Geology*, 42(6), 535–538. <https://doi.org/10.1130/G35327.1>
- Grujic, D., Warren, C. J., & Wooden, J. L. (2011). Rapid synconvergent exhumation of Miocene-aged lower orogenic crust in the eastern Himalaya. *Lithosphere*, 3(5), 346–366. <https://doi.org/10.1130/l1154.1>
- Hacker, B. R., & Christie, J. M. (1990). Brittle/ductile and plastic/cataclastic transitions in experimentally deformed and metamorphosed amphibolite. *Geophysical Monograph Series*, 127–147. <https://doi.org/10.1029/GM056p0127>
- Hacker, B. R., Kelemen, P. B., & Behn, M. D. (2015). Continental lower crust. *Annual Review of Earth and Planetary Sciences*, 43(1), 167–205. <https://doi.org/10.1146/annurev-earth-050212-124117>
- Hacker, B. R., Ritzwoller, M. H., & Xie, J. (2014). Partially melted, mica-bearing crust in central Tibet. *Tectonics*, 33(7), 1408–1424. <https://doi.org/10.1002/2014TC003545>
- Henriet, M., Avouac, J.-P., & Bills, B. G. (2019). Crustal rheology of southern Tibet constrained from lake-induced viscoelastic deformation. *Earth and Planetary Science Letters*, 506, 308–322. <https://doi.org/10.1016/j.epsl.2018.11.014>
- Hou, Z. Q., Zhou, Y., Wang, R., Zheng, Y. C., He, W. Y., Zhao, M., et al. (2017). Recycling of metal-fertilized lower continental crust: Origin of non-arc au-rich porphyry deposits at cratonic edges. *Geology*, 45(6), 563–566. <https://doi.org/10.1130/g38619.1>
- Hu, H., Dai, L., Li, H., Sun, W., & Li, B. (2018). Effect of dehydrogenation on the electrical conductivity of Fe-bearing amphibole: Implications for high conductivity anomalies in subduction zones and continental crust. *Earth and Planetary Science Letters*, 498, 27–37. <https://doi.org/10.1016/j.epsl.2018.06.003>
- Huang, B., Zhang, B., Zhang, J., Liu, S., Zhang, L., Ma, W., et al. (2022). Crustal anisotropy and deformation of the southeastern Tibetan Plateau revealed by seismic anisotropy of mylonitic amphibolites. *Journal of Structural Geology*, 159, 104605. <https://doi.org/10.1016/j.jsg.2022.104605>
- Huet, B., Yamato, P., & Grasemann, B. (2014). The Minimized Power Geometric model: An analytical mixing model for calculating polyphase rock viscosities consistent with experimental data. *Journal of Geophysical Research: Solid Earth*, 119(4), 3897–3924. <https://doi.org/10.1002/2013jb010453>

- Ji, S., Wirth, R., Rybacki, E., & Jiang, Z. (2000). High-temperature plastic deformation of quartz-plagioclase multilayers by layer-normal compression. *Journal of Geophysical Research: Solid Earth*, 105(B7), 16651–16664. <https://doi.org/10.1029/2000jb900130>
- Ji, S. C., Shao, T. B., Michibayashi, K., Oya, S., Satsukawa, T., Wang, Q., et al. (2015). Magnitude and symmetry of seismic anisotropy in mica- and amphibole-bearing metamorphic rocks and implications for tectonic interpretation of seismic data from the southeast Tibetan plateau. *Journal of Geophysical Research: Solid Earth*, 120(9), 6404–6430. <https://doi.org/10.1002/2015JB012209>
- Johnson, T. E., Brown, M., Gardiner, N. J., Kirkland, C. L., & Smithies, R. H. (2017). Earth's first stable continents did not form by subduction. *Nature*, 543(7644), 239–242. <https://doi.org/10.1038/nature21383>
- Kern, H., Gao, S., & Liu, Q.-S. (1996). Seismic properties and densities of middle and lower crustal rocks exposed along the North China Geoscience Transect. *Earth and Planetary Science Letters*, 139(3), 439–455. [https://doi.org/10.1016/0012-821X\(95\)00240-D](https://doi.org/10.1016/0012-821X(95)00240-D)
- Ko, B., & Jung, H. (2015). Crystal preferred orientation of an amphibole experimentally deformed by simple shear. *Nature Communications*, 6(1), 6586. <https://doi.org/10.1038/ncomms7586>
- Kohlstedt, D. L., Evans, B., & Mackwell, S. J. (1995). Strength of the lithosphere: Constraints imposed by laboratory experiments. *Journal of Geophysical Research: Solid Earth*, 100(B9), 17587–17602. <https://doi.org/10.1029/95jb01460>
- Lee, A. L., Stünitz, H., Soret, M., & Battisti, M. A. (2022). Dissolution precipitation creep as a process for the strain localisation in mafic rocks. *Journal of Structural Geology*, 155, 104505. <https://doi.org/10.1016/j.jsg.2021.104505>
- Li, W., Zhang, J., Wang, X., Wang, Y., Wu, X., & Hu, Z. (2020). Petrofabrics and seismic properties of himalayan amphibolites: Implications for a thick anisotropic deep crust beneath southern Tibet. *Journal of Geophysical Research: Solid Earth*, 128(8), 1–14. <https://doi.org/10.1029/2019jb018700>
- Liu, H., & Niu, F. (2012). Estimating crustal seismic anisotropy with a joint analysis of radial and transverse receiver function data. *Geophysical Journal International*, 188(1), 144–164. <https://doi.org/10.1111/j.1365-246X.2011.05249.x>
- Lloyd, G. E., Butler, R. W. H., Casey, M., & Mainprice, D. (2009). Mica, deformation fabrics and the seismic properties of the continental crust. *Earth and Planetary Science Letters*, 288(1–2), 320–328. <https://doi.org/10.1016/j.epsl.2009.09.035>
- Mackwell, S. J., Zimmerman, M. E., & Kohlstedt, D. L. (1998). High-temperature deformation of dry diabase with application to tectonics on Venus. *Journal of Geophysical Research: Solid Earth*, 103(B1), 975–984. <https://doi.org/10.1029/97jb02671>
- Mansard, N., Stünitz, H., Raimbourg, H., Précigout, J., Plunder, A., & Nègre, L. (2020). Relationship between microstructures and resistance in mafic assemblages that deform and transform. *Solid Earth*, 11(6), 2141–2167. <https://doi.org/10.5194/se-11-2141-2020>
- Moschetti, M. P., Ritzwoller, M. H., Lin, F., & Yang, Y. (2010). Seismic evidence for widespread western-us deep-crustal deformation caused by extension. *Nature*, 464(7290), 885–889. <https://doi.org/10.1038/nature08951>
- Okazaki, K., & Hirth, G. (2016). Dehydration of lawsonite could directly trigger earthquakes in subducting oceanic crust. *Nature*, 530(7588), 81–84. <https://doi.org/10.1038/nature16501>
- Phillips, N. J., & Ji, S. (2021). Constraining the ductile deformation mechanisms of garnet across pressure-temperature space. *Journal of Structural Geology*, 148, 104356. <https://doi.org/10.1016/j.jsg.2021.104356>
- Rippe, D., & Unsworth, M. (2010). Quantifying crustal flow in Tibet with magnetotelluric data. *Physics of the Earth and Planetary Interiors*, 179(3–4), 107–121. <https://doi.org/10.1016/j.pepi.2010.01.009>
- Rooney, T. P., Riecker, R. E., & Gavasci, A. T. (1975). Hornblende deformation features. *Geology*, 3(7), 364–366. [https://doi.org/10.1130/0091-7613\(1975\)3<364:HDF>2.0.CO;2](https://doi.org/10.1130/0091-7613(1975)3<364:HDF>2.0.CO;2)
- Royden, L. H., Burchfiel, B. C., King, R. W., Wang, E., Chen, Z., Shen, F., & Liu, Y. (1997). Surface deformation and lower crustal flow in eastern Tibet. *Science*, 276(5313), 788–790. <https://doi.org/10.1126/science.276.5313.788>
- Rudnick, R. L., & Gao, S. (2014). Composition of the continental crust. *Treatise on geochemistry*, 1–51. <https://doi.org/10.1016/b978-0-08-095975-7.00301-6>
- Rybacki, E., & Dresen, G. (2000). Dislocation and diffusion creep of synthetic anorthite aggregates. *Journal of Geophysical Research: Solid Earth*, 105(B11), 26017–26036. <https://doi.org/10.1029/2000jb900223>
- Ryder, I., Wang, H., Bie, L., & Rietbrock, A. (2014). Geodetic imaging of late postseismic lower crustal flow in Tibet. *Earth and Planetary Science Letters*, 404, 136–143. <https://doi.org/10.1016/j.epsl.2014.07.026>
- Shinevar, W. J., Behn, M. D., & Hirth, G. (2015). Compositional dependence of lower crustal viscosity. *Geophysical Research Letters*, 42(20), 8333–8340. <https://doi.org/10.1002/2015gl065459>
- Shinevar, W. J., Jagoutz, O., & VanTongeren, J. A. (2021). Gore mountain garnet amphibolite records UHT conditions: Implications for the rheology of the lower continental crust during orogenesis. *Journal of Petrology*, 62(4). <https://doi.org/10.1093/petrology/egab007>
- Skrotzki, W. (1992). Defect structure and deformation mechanisms in naturally deformed hornblende. *Physica Status Solidi*, 131(2), 605–624. <https://doi.org/10.1002/pssa.2211310232>
- Sloan, R. A., Jackson, J. A., McKenzie, D., & Priestley, K. (2011). Earthquake depth distributions in central Asia, and their relations with lithosphere thickness, shortening and extension. *Geophysical Journal International*, 185(1), 1–29. <https://doi.org/10.1111/j.1365-246X.2010.04882.x>
- Stokes, M. R., Wintsch, R. P., & Southworth, C. S. (2012). Deformation of amphibolites via dissolution-precipitation creep in the middle and lower crust. *Journal of Metamorphic Geology*, 30(7), 723–737. <https://doi.org/10.1111/j.1525-1314.2012.00989.x>
- Tapponnier, P., Zhiqin, X., Roger, F., Meyer, B., Arnaud, N., Wittlinger, G., & Jingsui, Y. (2001). Oblique stepwise rise and growth of the Tibet Plateau. *Science*, 294(5547), 1671–1677. <https://doi.org/10.1126/science.105978>
- Tommasi, A., Langone, A., Padron-Navarta, J. A., Zanetti, A., & Vauchez, A. (2017). Hydrous melts weaken the mantle, crystallization of amphibole and phlogopite does not: Insights from a petrostructural study of the Finero peridotites, Southern Alps. *Earth and Planetary Science Letters*, 477, 59–72. <https://doi.org/10.1016/j.epsl.2017.08.015>
- Turner, S., Arnaud, N., Liu, J., Rogers, N., Hawkesworth, C., Harris, N., et al. (1996). Post-collision, shoshonitic volcanism on the Tibetan Plateau: Implications for convective thinning of the lithosphere and the source of ocean island basalts. *Journal of Petrology*, 37(1), 45–71. <https://doi.org/10.1093/petrology/37.1.45>
- Voegelé, V., Ando, J., Cordier, P., & Liebermann, R. (1998). Plastic deformation of silicate garnets: I. High-Pressure experiments. *Physics of the Earth and Planetary Interiors*, 108(4), 305–318. [https://doi.org/10.1016/S0031-9201\(98\)00110-1](https://doi.org/10.1016/S0031-9201(98)00110-1)
- Wang, C. Y., Chen, W. P., & Wang, L. P. (2013). Temperature beneath Tibet. *Earth and Planetary Science Letters*, 375, 326–337. <https://doi.org/10.1016/j.epsl.2013.05.052>
- Wang, G., Thybo, H., & Artemieva, I. M. (2021). No mafic layer in 80 km thick Tibetan crust. *Nature Communications*, 12(1), 1069. <https://doi.org/10.1038/s41467-021-21420-z>
- Wang, X., Zhang, J., Rushmer, T., Adam, J., Turner, S., & Xu, W. (2019). Adakite-like potassio magmatism and crust-mantle interaction in a postcollisional setting: An experimental study of melting beneath the Tibetan Plateau. *Journal of Geophysical Research: Solid Earth*, 124(12), 12782–12798. <https://doi.org/10.1029/2019jb018392>

- Wang, X., Zhang, J., Tommasi, A., Jing, Z., & Yuan, M. (2021). Microstructure and seismic properties of amphibole-rich rocks from the deep crust in southern Tibet. *Tectonophysics*, 811, 228869. <https://doi.org/10.1016/j.tecto.2021.228869>
- Wilks, K. R., & Carter, N. L. (1990). Rheology of some continental lower crustal rocks. *Tectonophysics*, 182(1–2), 57–77. [https://doi.org/10.1016/0040-1951\(90\)90342-6](https://doi.org/10.1016/0040-1951(90)90342-6)
- Wu, C., Tian, X., Xu, T., Liang, X., Chen, Y., Taylor, M., et al. (2019). Deformation of crust and upper mantle in central Tibet caused by the northward subduction and slab tearing of the Indian lithosphere: New evidence based on shear wave splitting measurements. *Earth and Planetary Science Letters*, 514, 75–83. <https://doi.org/10.1016/j.epsl.2019.02.037>
- Zhang, J., Chang, J., Wang, R., & Audéat, A. (2022). Can post-subduction porphyry cu magmas form by partial melting of typical lower crustal amphibole-rich cumulates? Petrographic and experimental constraints from samples of the Kohistan and gangdese arc roots. *Journal of Petrology*, 63(11). <https://doi.org/10.1093/petrology/egac101>
- Zhang, J., & Green, H. W. (2007). Experimental investigation of eclogite rheology and its fabrics at high temperature and pressure. *Journal of Metamorphic Geology*, 25(2), 97–115. <https://doi.org/10.1111/j.1525-1314.2006.00684.x>
- Zhou, J.-S., Yang, Z.-S., Hou, Z.-Q., & Wang, Q. (2020). Amphibole-rich cumulate xenoliths in the zhazhalong intrusive suite, gangdese arc: Implications for the role of amphibole fractionation during magma evolution. *American Mineralogist*, 105(2), 262–275. <https://doi.org/10.2138/am-2020-7199>